

Image-based BRDF Acquisition for Non-spherical Objects

Tsung-Yi Wu

Wan-Chun Ma

Yung-Yu Chuang

Bing-Yu Chen

Ming Ouhyoung

National Taiwan University

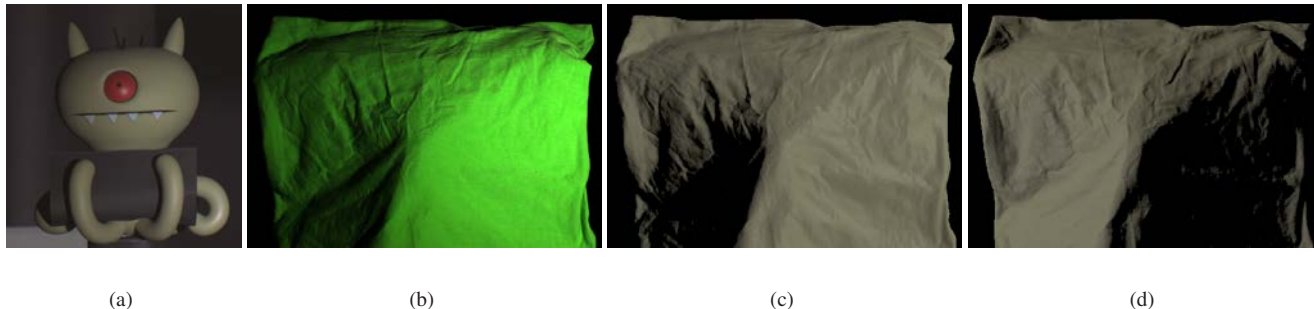


Figure 1: An overview of image-based BRDF acquisition. (a) An object of arbitrary shape that we will capture the BRDF from. (b) A real photograph of cloth. (c) A synthetic image of the same cloth, but applied with the BRDF captured from (a). (d) A synthetic image under another lighting condition.

Abstract

In order to create photorealistic images, we need to know how light is reflected from different materials. The bidirectional reflectance distribution functions (BRDF) plays an important role in modeling the reflectance of materials. This paper presents a framework for extracting BRDF samples from multiple photographs, which are taken from the same viewpoint but under different lighting directions, of an arbitrary object. After collecting samples, we use a smoothing interpolation to approximate the complete BRDF from the measured samples.

1 Introduction

It is an important issue to model and measure how light is reflected from surfaces of an object in computer graphics and computer vision. Take the movie "The Matrix Reloaded" as an example, the special effect team tried to measure true reflectance of certain materials such as the actors' costumes. The measured data is then used in their rendering framework for realistic renderings [Borshukov 2003].

Bidirectional reflectance distribution functions(BRDFs) are widely-used models for describing how the light is reflected when it interacts with the surface of a certain material. Generally, a BRDF is a function which returns the ratio of incoming and outgoing energy relative to a local orientation at the contact point. Additionally, the BRDF is wavelength dependent: lights of different wavelengths may have different reflectivities. In practice, we usually represent the wavelength term by using only three color (red, green, and blue). Thus, for each color channel, a BRDF can be defined as a four dimensional function, which is written as $\mu(\omega_i, \omega_o)$, where ω_i is the incoming light direction and ω_o is the outgoing direction. Both of ω_i and ω_o are defined in a polar coordinate system. Therefore, a BRDF is defined as the ratio of the amount of light reflected in direction ω_i to the amount of light illuminate at the surface from direction ω_o . In this paper, we

use a subclass of BRDFs called isotropic BRDFs which ignores the rotations about the surface normal and the dimension of BRDFs is reduced to three.

1.1 Overview

There are several ways to acquire BRDFs. To simplify the problem, many methods require that the shape of the target object is known in advance. Furthermore, many image-based BRDF acquisition methods can only work for flat or spherical objects. However, in real world, most objects are not flat or spherical. Hence, it is not reasonable to make these objects into flat or spherical in order to get their BRDFs. Take human skin as an example, the shape of face is neither totally flat nor spherical. Furthermore, since it is impossible to change the shape of the face, we need to develop another method which allows BRDF acquisition for objects of arbitrary shapes. The key idea is, once the shape of the object is found (or estimated), we can straightly solve the reflectance of the material over the object. Therefore, we can divide this problem into two parts: one is the recovery (estimation) of the shape, and the other is the measurement of reflectance.

This paper is organized as follows. In Section 2, we briefly introduce the related work on modeling and measuring of reflectance. In Section 3, we describe the acquisition process, which contains an introduction of the devices we used and how to perform lighting calibration. In Section 4, we describe how to convert the measured data into BRDFs in different coordinate systems. In Section 5, in order to recover the whole BRDF from scattered samples, we describe an interpolation method which invokes *approximate nearest neighbor* (ANN) for fast search. In Section 6, we demonstrate several results including objects with single or multiple materials. Finally, Section 7 summarizes our contributions and states the future work.



Figure 2: A snapshot of our acquisition system.

2 Related Work

Sometimes we need to obtain direct measurements of given materials. Traditionally, BRDFs are measured by a gonireflectometer which consists of a light source and a detector. A BRDF sample is measured at each movement of the light source and the detector. It is very time consuming sometimes impractical to measure dense data using this device. To improve the efficiency of measurement device, Ward [1992] measured the BRDF by using a hemisphere mirror and a fish-eye lens to gather BRDF samples from a flat material. Dana [2001] used an off-axis parabolic mirror to obtain BRDF samples. Currently, image-based BRDF acquisition becomes more and more popular. Lots of the BRDF samples can be acquired from a single image. Marschner *et al.* [1999] directly measured an object with known shape. For each acquired image, lots of the BRDF samples are acquired and the efficiency is greatly improved. Matusik *et al.* [2003a; 2003b] acquired dense BRDF samples from spherical objects of more than 100 materials. The whole process only takes about 3 hours to acquire the BRDF for each material.

3 Data Acquisition

In this section, we describe the BRDF data acquisition process of our system. For each capture session, we need to calibrate relative intensity and direction of each light. After lighting calibration, we can take multiple images under different lighting conditions by moving the light sources. Our system assumes that the camera is orthographic and the light sources are distant lights. Each pixel in the captured images can be regarded as a BRDF sample.

3.1 Acquiring Images

Our acquisition system consists of a Canon EOS 20D digital camera controlled by a computer and a light stand with three LED light sources mounted on it. A real photograph of our system is shown in Figure 2. The distance from the object to the camera is about 2.5 meters and the distance from the object to the light stand is about 1.5 meters. During the acquisition, we move the light stand around the object and capture images. We capture total of 36 images for each object, although these images may not all be used. For the

objects with high reflectivity, we need to capture multiple exposures of images to construct a high dynamic range image for each lighting direction. On the contrary, we only capture low dynamic range images for diffuse objects since LDR images are already accurate enough. Upon finishing the acquisition, all the images captured are adjusted by the scaling factors recovered by light calibration.

3.2 Light Calibration

Before proceeding to the acquisition process, the directions of the light sources to the object and their relative intensities need to be calibrated first. We use the method which is proposed by Goldman *et al.* [2004] to calibrate the light sources. Two spheres are used for calibration: a steel one and a styrofoam one coated with white diffuse paint. For each light source, we capture one images of a steel sphere and another image of a styrofoam sphere. The image of steel sphere is used to find the light directions and the image of styrofoam sphere is used to figure out the relative intensities of light sources.

Lighting Direction: We locate the brightest pixel p_{max} in the i_{th} image, \mathbf{I}_i , to calculate the direction of the light source. Since the object is sphere and the camera is orthographic, we can compute the normal vector at p_{max} , which is denoted as $\mathbf{n}_{p_{max}} = (n_x, n_y, n_z)$. The lighting direction, \mathbf{L}_i , is recovered by reflecting the viewing vector about $\mathbf{n}_{p_{max}}$. Since the viewing vector is $(0, 0, 1)$, then

$$\mathbf{L}_i = (2n_x n_z, 2n_y n_z, 2n_z^2 - 1) \quad (1)$$

Lighting Intensity: If the lighting direction \mathbf{L}_i is known, the intensity of the diffuse sphere at pixel p in image \mathbf{I}_i is $\mathbf{I}_{(i,p)} = \mathbf{E}_i \rho (\mathbf{n}_p \cdot \mathbf{L}_i)$, where ρ is the diffuse albedo and \mathbf{E}_i is the lighting intensity. We can recover the relative intensity by solving the following equation

$$\mathbf{E}_i \rho = \frac{\sum_p \mathbf{I}_{(i,p)}}{\sum_p \mathbf{n}_p^T \mathbf{L}_i} \quad (2)$$

Because the paint used on the styrofoam sphere may not be totally diffuse, We can not apply all the pixels to solve $\mathbf{E}_i \rho$. For each pixel p with its normal \mathbf{n}_p and the lighting direction \mathbf{L}_i , three rules are used to remove outliers. The pixel p is removed when

1. $\mathbf{n}_p^T \mathbf{L}_i$ is not in the interval $[t_1, t_2]$,
2. The angle between the viewing vector \mathbf{V} and the reflection vector \mathbf{R} is above t_3 ,
3. The intensity of the point $\mathbf{I}_{(i,p)}$ is below t_4 ,

where t_1, t_2, t_3 and t_4 are thresholds set empirically. The rules 1 and 2 are used to remove pixels in the specular highlights and the rule 3 is used to remove dark pixels. After light calibration is done, scaling factors of three color channels are known and images are scaled accordingly.

4 Arranging BRDF Measurements from Acquired Images

4.1 Computing Surface Orientation

To convert the captured samples into BRDF data, we need to compute normals of the surface. Here, we used standard Lambertian photometric stereo [Woodham 1980]. Although this method can not work well if there are specular highlights or shadows, we get

around these limitations by taking multiple images into consideration and rejecting highlight and shadow pixels.

Suppose we have n images of an arbitrary object taken under various lighting conditions. Let $\mathbf{I}_p = [\mathbf{I}_{(1,p)}, \mathbf{I}_{(2,p)}, \dots, \mathbf{I}_{(n,p)}]^T$ be a vector of the intensity at the point p and $\mathbf{L} = [\mathbf{L}_1, \mathbf{L}_2, \dots, \mathbf{L}_n]^T$. Assuming that the material is diffuse, the following equation holds:

$$\mathbf{I}_p = \rho \mathbf{L}^T \mathbf{n}_p \quad (3)$$

Then we can solve the resulting linear system to obtain $\rho \mathbf{n}_p = \mathbf{L}^{-1} \mathbf{I}_p$. Because \mathbf{n}_p is a unit vector, we have $\rho = |\mathbf{L}^{-1} \mathbf{I}_p|$ and $\mathbf{n}_p = \frac{1}{\rho} \mathbf{L}^{-1} \mathbf{I}_p$. In our implementation, because we always have more than three images to recover the normals, we use SVD to solve \mathbf{n}_p and the problem becomes a least-square fitting to a set of linear equations.

4.2 Outlier removal

To obtain good surface normals, we have to remove pixels in specular highlight or shadows. The simplest method is to let users manually choose intensity thresholds to remove the outliers. However, the quality of the normal map will totally depend on these thresholds. To improve the quality, we have tried other two methods: two-steps outlier removal and RANSAC method.

Two-steps Outlier Removal. This method is based on finding the best pixel combination. We need at least three measurements to solve Equation 3. There are C_3^n combinations if we randomly choose three measurements from \mathbf{I}_p . The first step is, for each combination \mathbf{C}_j , $1 \leq j \leq C_3^n$, we compute the diffuse factor ρ_j . The \mathbf{C}_j is not valid if ρ_j is not within a given range. After removing the outliers, we apply Lambertian photometric stereo on the remaining pixels to find the normal \mathbf{n}_p and the diffuse factor ρ . Although we get a recommendable set of pixels for normal recovery, there may still be outliers in this set. Thus, the second step is to remove these outliers by examining how far away they are from the line created at the previous step. Finally, we use Lambertian photometric stereo again to get the final result.

Random Sample Consensus Algorithm. Random sample consensus algorithm (RANSAC) [Fischler and Bolles 1981] is an algorithm for robust fitting of models in the presence of outliers. Since our inputs are a small number of images, we modify the original RANSAC algorithm to fit our requirements. First, similar to the two-steps outlier removal, we choose three pixels at one time and there are totally C_3^n combinations to be examined instead of choosing three pixels randomly. The algorithm includes the following steps:

1. For each combination \mathbf{C}_j of measurements, we fit a line to it. Then, we compute the error term which is the sum of the distances of all measurements to the fit line.
2. We use the combination which has minimum error as the best initial fit. Then we check on all the pixels and find the valid pixels which have small enough error within a given threshold.
3. We use photometric stereo again to recover the normal from these valid pixels as the final result.

For every object, we generate three normal maps using these three methods and choose the best one to use. However, in some cases, highlight pixels still affect the result and are not removed totally. For these cases, we just manually select these regions where highlight pixels exist and estimate normals in these regions by smoothing out neighboring normals.

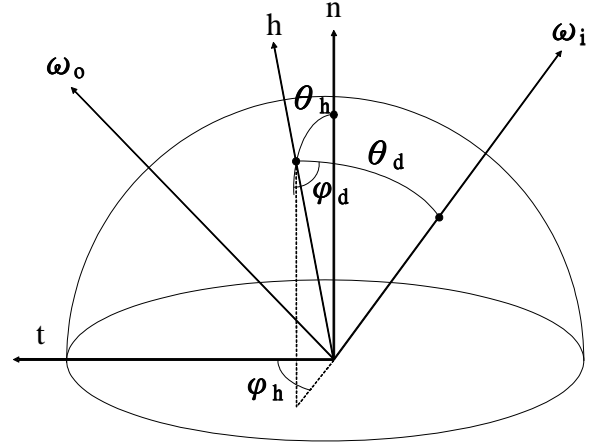


Figure 3: Rusinkiewicz coordinate system.

4.3 Segmentation for Objects with Multiple Materials

In general, the objects we desire to capture may consist of multiple materials. We design a method to capture multiple materials from a single object at once. In our system, we segment the object into several regions manually according to their diffuse colors. We also assume that the boundaries of the material regions are distinct enough to simplify the problem. However, there are always pixels at the boundaries of the regions which may be composed of multiple materials. Thus, we separate each region into two parts: inner part and boundary part, and only take inner parts for BRDF acquisition. This assumption does limit the scope of our system from measuring objects with very complex materials on their surfaces and need to be addressed in the future.

4.4 Coordinate System

After image acquisition and recovery of normal maps, we have to convert the captured samples into BRDF data. The goal is, for each sample, to use the normal map to find the corresponding location in the BRDF space, and put the data into a BRDF table.

Natural Coordinate. For isotropic BRDFs, the BRDF values will be the same when rotating about the normal of the surface. Based on this characteristic, we can define isotropic BRDFs using natural coordinate system as

$$\mu_n(\theta_i, \theta_o, \phi_d), \quad (4)$$

where $\phi_d = \phi_i - \phi_o$ is used to represent the rotation invariant. Here we describe how to convert captured data into a BRDF in natural coordinate system. For a BRDF sample at pixel p with the normal $\mathbf{n}_p = (n_x, n_y, n_z)$ under the conditions that the lighting direction is \mathbf{L} and the viewing direction is \mathbf{V} , we can derive the new lighting and viewing direction \mathbf{L}' and \mathbf{V}' relative to \mathbf{n}_p by the following equation:

$$\mathbf{L}' = R_{u, \arccos(n_z)} \mathbf{L} \quad (5)$$

$$\mathbf{V}' = R_{u, \arccos(n_z)} \mathbf{V} \quad (6)$$

where $N = (0, 0, 1)$ is the up vector in the tangent space, $u = \mathbf{n}_p \times N$, $R_{u, \theta}$ is a 3×3 transformation matrix that rotates by an angle θ about an arbitrary direction u . Then \mathbf{L}' and \mathbf{V}' are further transformed into

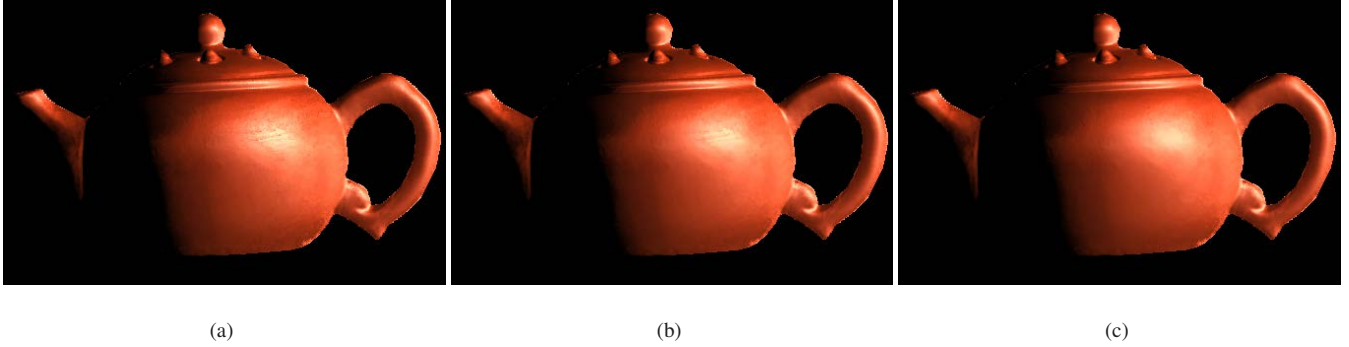


Figure 4: Results of using different k nearest neighbors. (a) $k = 5$. (b) $k = 25$. (c) $k = 100$.

polar coordinates, $\omega'_i = (\theta_i, \phi_i)$ and $\omega'_o = (\theta_o, \phi_o)$. We then assign the BRDF sample to the $\mu_n(\theta_i, \theta_o, \phi_d)$.

Rusinkiewicz Coordinate: Although natural coordinate system can easily be made out, there is a disadvantage of using it. For materials with specular characteristics, features of specular peaks can not be preserved by interpolation methods because we only have sparsely sampled BRDF data. Thus, we use a different coordinate system which is proposed by Rusinkiewicz [1998], which is shown in Figure 3. Unlike natural coordinate system, a BRDF is parameterized as a function of a halfway vector and a difference vector:

$$\mu_r(\theta_h, \theta_d, \phi_d). \quad (7)$$

With this coordinate, specular reflection will be aligned with the θ_d axis and the shape of peaks will be preserved while using interpolation on the sampled data. Converting sample data into Rusinkiewicz coordinate is also quite simple. Given the lighting direction \mathbf{L} and viewing direction \mathbf{V} , the halfway vector \mathbf{H} is derived by

$$\mathbf{H} = \frac{\mathbf{L} + \mathbf{V}}{|\mathbf{L} + \mathbf{V}|}, \quad (8)$$

and the difference vector \mathbf{D} is derived by

$$\mathbf{D} = R_{v, -\theta_h} R_{u, -\phi_h} \mathbf{L}, \quad (9)$$

where where $T = (0, 1, 0)$ is the left vector in the tangent space, $v = \mathbf{n}_p \times T$, and $u = \mathbf{n}_p \times Z$. Then, \mathbf{H} and \mathbf{D} are further transformed into polar coordinates, $\omega_h = (\theta_h, \phi_h)$ and $\omega_d = (\theta_d, \phi_d)$. We then assign the BRDF sample to the $\mu_r(\theta_h, \theta_d, \phi_d)$. There is another advantage of using Rusinkiewicz coordinate. In our system, we assume that the camera is orthogonal and the light sources are parallel projected. Hence, all the pixels in the same image will have the same θ_d , since $\theta_d = \arccos(\mathbf{H}^T \mathbf{L})$. Therefore, we can treat each acquired image as a ‘‘slice’’ in the BRDF space.

5 Interpolation Scheme

If we acquire BRDF samples from spherical objects similar to the work by Matusik *et al.* [2003a; 2003b], we can get high quality measurements since the shape of the object is known and we can acquire all possible normals from a sphere. The major difficulty we face is that both shape and reflectance model are unknown. In previous two sections, we have described how to recover the shape of the object from photographs and how to convert the captured data into different BRDF coordinate system. Now the problem is, since we

have scattered BRDF data, we need to interpolate the data to recover the complete BRDF. Scattered data interpolation techniques are very useful in many areas, such as chemistry, physics, and engineering. In computer graphics, it also can be used for model reconstruction from scanned data points [Park and Lee 1997]. There are many ways to interpolate scattered data. Lee *et al.* [1997] proposed an algorithm for interpolation and approximation using multilevel B-splines. Radial basis functions (RBFs) are also used for interpolation and approximation of scattered data [Floater and Iske 1996].

5.1 The Epanechnikov Kernel

In our system, a local smoothing method is used to interpolate the acquired data. We treat a BRDF as a probability density function and the measured data are sample points of the probability density function. To estimate the complete function, we use a non-parametric estimator called Epanechnikov kernel [Simonoff 1996]. This kernel is a discontinuous parabola function of the following form:

$$h(x) = \begin{cases} \frac{3}{4}(1-u^2) & -1 < u < 1 \\ 0 & \text{otherwise,} \end{cases} \quad (10)$$

where $u = \frac{x-x_i}{h}$, h is the bandwidth and x_i are the values of the variable in the data. In our system, we use the distance from input values to measured data as $x - x_i$, then we can interpolate BRDF values at any position.

5.2 Search Strategy

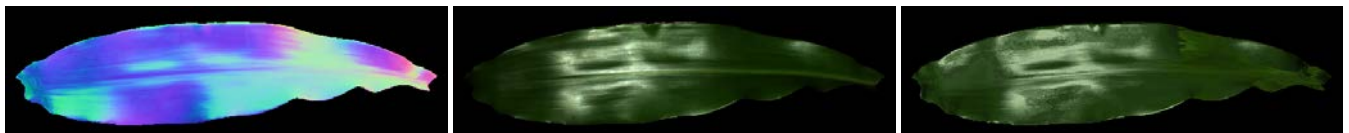
Originally, we need to do an exhaustive search on all the BRDF data to find the interpolated result. But we find that it is not necessary to search every data point since most of them have no contribution to the interpolated value because of the bandwidth. Hence, to improve the performance of search, we used an approximated solution. We build an ANN search structure [Arya *et al.* 1998] for the data and query the value through it. We only find the k nearest neighbors for interpolation, and the bandwidth will automatically changed according the minimum and maximum distances of the data to ensure that we can always find an interpolated value. Figure 4 shows the results using different k . We can get a smoother result by choosing a larger k , but it also takes longer to compute.



(a)



(b)



(c)



(d)

Figure 5: Results of image-based BRDF acquisition. At the left, the recovered normal map; at the center, one of the source image; at the right, a synthetic image rendered under the same lighting condition. (a) A red teapot. (b) A brown teapot, (c) A leaf. (d) A T-shirt.

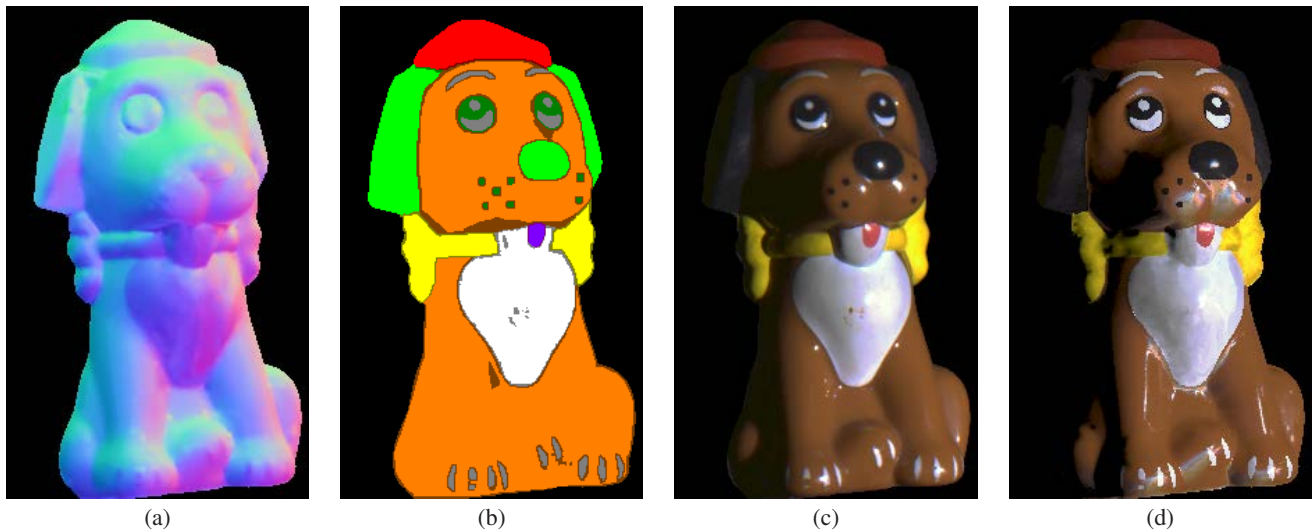


Figure 6: Results of image-based BRDF acquisition for a object with multiple materials. (a) The recovered normal map. (b) The segmentation map. (c) One of the source image. (d) A synthetic image rendered under the same lighting condition.

6 Results

In this section, we present results using the technique we have described including captured images, corresponding estimated normal maps, and the reconstructed images. We first use our system to retrieve BRDF from objects with a single material. Figure 5 (a) and (b) shows the results of acquisition and reconstruction of BRDFs for two teapots. From left to right, we show the estimated normal map, one of the input image for some lighting direction and the reconstructed image using the recovered normal map and interpolated BRDF data under the same lighting direction. It is noticeable that, due to the shape of the teapots, they cast self-shadows on their surface. Our algorithm can detect self-shadows and do not take these illegal samples into account. Figure 5 (c) and (d) show more results of acquisition and reconstruction of BRDFs for a leaf and a green T-shirt. To test out system on objects with multiple materials, we also captured a plastic dog, which is shown in Figure 6. Because we use a smoothing method to retrieve BRDF values, the brightness of highlight pixels may be darker than captured image. The RANSAC algorithm performs better because there are both white and black regions and it is not easy to choose suitable thresholds for other two methods.

To demonstrate the capability of material transfer, we capture a plastic monster doll (Figure 1(a)) and acquire its grey diffuse material. We then render the captured material with the recovered normal map of a cloth (Figure 1(b)) to make the cloth plastic as shown in Figure 1(c) and (d). The acquired materials can also be rendered onto synthetic objects. Figure 7(a) is the normal map for a geometric model of a statue. We map the acquired material onto its surface to give it different looks like grey plastic (Figure 7(b)), green cloth (Figure 7(c)) and leaf under two different lighting conditions (Figure 7(d) and (e)).

7 Conclusions and Future Work

To create photorealistic images, it is better to use measured data instead of an analytical model to preserve the details of the material. In this paper, we build an image-based acquisition system to

measure BRDFs from real objects. During the experiments, we actually acquire BRDFs from 6 objects. Although there are still some flaws in the results due to the error of light calibration and surface orientation estimator, the system itself is robust and easy to use. A local smoothing method is used to reduce the noise in data acquisition to create images of different viewpoints from original captured images. In the future, we would like to explore the following directions.

Precise Surface Normal Estimation. So far, the reconstructed BRDF can still not be very accurate at highlight pixels because the estimated normal maps are not accurate enough especially near the edges of the objects. Hertzmann *et al.*[2003] use a captured reference sphere to estimate the normals of the object, but their method suffers from the existence of self-shadow. We may solve this problem by using a partial matching algorithm in the future. Mallick *et al.*[2005] also propose a method to reconstruct specular surfaces without explicit reflectance model or reference objects.

BRDF Measurement for Objects with Complex Shapes. To improve the generality of this system, the ability to measure BRDF data from complex objects is necessary. How can we acquire the BRDF data from a strange-shaped object with multiple materials? The existence of self-shadows is a thorny problem for us to cluster the materials. All we need is a segmentation algorithm to separate different materials even if there are shadow or highlight pixels.

Reflectance Representation. If we want to use the measured BRDF data for rendering, we need to look it up in the BRDF database and find the query result for each pixel. This process is really time-consuming and hence not suitable for real-time rendering. Thus, we would like to reduce the amount of data to save both storage space and computation time. Principal components analysis (PCA) might be a good starting point to compress the BRDF data.

Acknowledgement

This work was partially supported by the CIET-NTU(MOE) and National Science Council of Taiwan under NSC93-2622-E-002-033, NSC93-2752-E-002-007-PAE, NSC93-2213-E-002-083, NSC93-2213-E-002-084 and NSC94-2213-E-002-051.

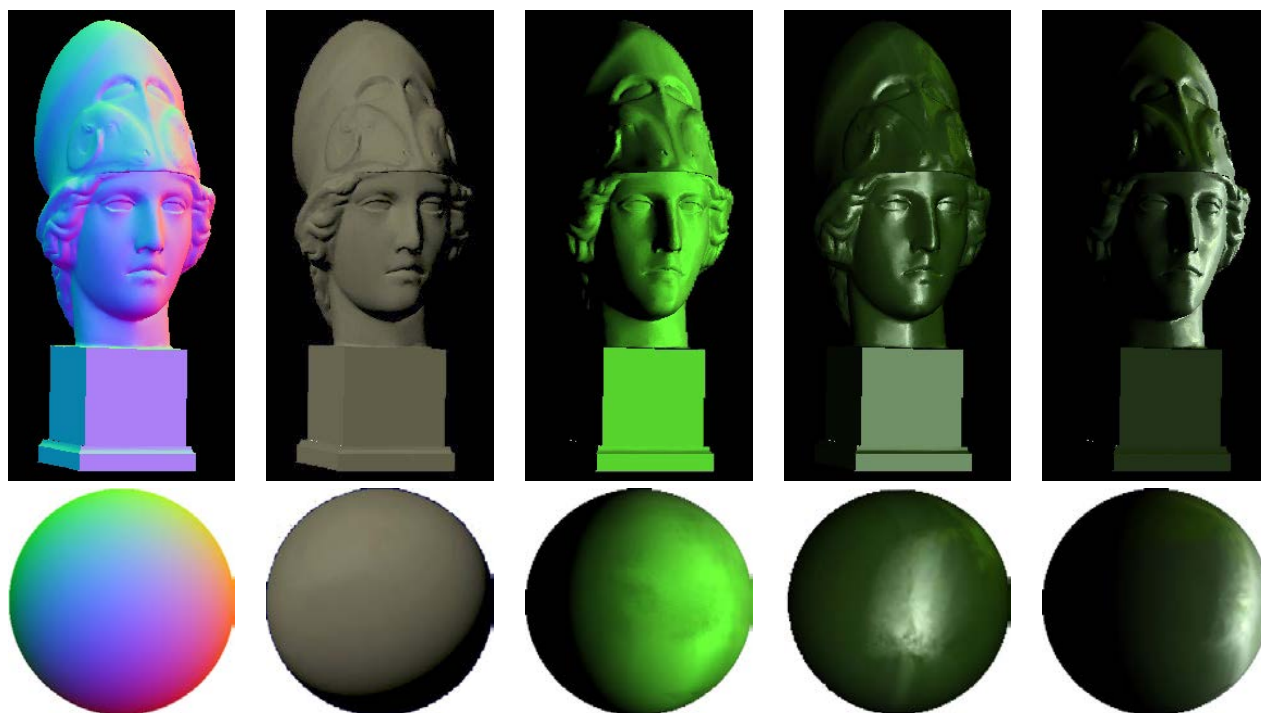


Figure 7: The top of (a) is the normal map for a geometric model of a statue. The bottom is the normal map for a sphere. We map the acquired material onto the surface of the statue to give it different looks of grey plastic (b), green cloth (c) and leaf under two different lighting conditions ((d) and (e)). The bottom shows the renderings of the reference balls of these materials.

References

- ARYA, S., MOUNT, D. M., NETANYAHU, N. S., SILVERMAN, R., AND WU, A. Y. 1998. An optimal algorithm for approximate nearest neighbor searching fixed dimensions. *Journal of the ACM* 45, 6, 891–923.
- BORSHUKOV, G. 2003. Measured brdf in film production: Realistic cloth appearance for “the matrix reloaded”.
- DANA, K. J. 2001. Brdf/btf measurement device. In *Proc. IEEE International Conference on Computer Vision (ICCV)*, 460–466.
- FISCHLER, M. A., AND BOLLES, R. C. 1981. Random sample consensus: A paradigm for model fitting with applications to image analysis and automated cartography. *Communications of the ACM* 24, 6, 381–395.
- FLOATER, M. S., AND ISKE, A. 1996. Multistep scattered data interpolation using compactly supported radial basis functions. *Journal of Computational and Applied Mathematics* 73, 1-2, 65–78.
- GOLDMAN, D. B., CURLESS, B., HERTZMANN, A., AND SEITZ, S. 2004. Shape and spatially-varying brdfs from photometric stereo. *UW-CSE-04-05-03*.
- HERTZMANN, A., AND SEITZ, S. 2003. Shape and materials by example: A photometric stereo approach. In *Proc. IEEE Conference on Computer Vision and Pattern Recognition (CVPR)*, 533–540.
- LEE, S., WOLBERG, G., AND SHIN, S. Y. 1997. Scattered data interpolation with multilevel b-splines. *IEEE Transaction on Visualization and Computer Graphics* 3, 3, 228–244.
- MALLICK, S. P., ZICKLER, T. E., KRIEGMAN, D. J., AND BELHUMEUR, P. N. 2005. Beyond lambert: Reconstructing specular surfaces using color. In *Proc. IEEE Conference on Computer Vision and Pattern Recognition (CVPR)*.
- MARSCHNER, S. R., WESTIN, S. H., LAFORTUNE, E. P. F., TORRANCE, K. E., AND GREENBERG, D. P. 1999. Image-based brdf measurement including human skin. In *Proc. Eurographics Workshop on Rendering*, 139–152.
- MATUSIK, W., PFISTER, H., BRAND, M., AND MCMILLAN, L. 2003. A data-driven reflectance model. *ACM Transactions on Graphics* 22, 3, 759–769.
- MATUSIK, W., PFISTER, H., BRAND, M., AND MCMILLAN, L. 2003. Efficient isotropic brdf measurement. In *Proc. Eurographics workshop on Rendering*, 241–247.
- PARK, I. K., AND LEE, S. U. 1997. Geometric modeling from scattered 3-d range data. In *Proc. International Conference on Image Processing (ICIP)*, 712–715.
- RUSINKIEWICZ, S. M. 1998. A new change of variables for efficient brdf representation. In *Proc. Eurographics Workshop on Rendering*, 11–12.
- SIMONOFF, J. S. 1996. *Smoothing Methods in Statistics*. Springer.
- WARD, G. J. 1992. Measuring and modeling anisotropic reflection. In *Proc. SIGGRAPH 1992*, 265–272.
- WOODHAM, R. J. 1980. Photometric method for determining surface orientation from multiple images. *Optical Engineering* 19, 1, 139–144.